Indian Journal of Pure & Applied Physics
Vol. 61, October 2023, pp. 840-845
DOI: 10.56042/ijpap.v61i10.2805

DFT Study of Hexagonal Boron Nitride Electronic Properties Using Different Types of Exchange Correlation Functionals

Issa Z Hassan[a*], Hassan A Kadhem[b] & Abdul Hakim Sh Mohammed[a]

[a]Department of Physics, College of Education, University of Kirkuk, Kirkuk 52001, Iraq

[b]Open Educational College, Kirkuk 52001, Iraq

Received 20 June 2023; accepted 4 August 2023

Density functional theory (DFT) description of electronic structure and related properties offer significant accuracy with low cost. Unfortunately, most of these calculations based on LDA and GGA Exchange-Correlation (XC) functionals are underestimating the energy band gap. Hybrid functionals seem promising candidates for band gap values enhancement. Hexagonal Boron Nitride (*h*-BN) is one of the important members of the graphene-like two-dimensional honeycomb structure family which is of great importance both for science and technology. Experimentally, there is convincing evidence for an indirect wide bandgap of about 6 eV. We present in this work a systematic DFT study using different types of Exchange-Correlation (XC) functionals to find out their accuracy to estimate the *h*-BN band gap along with its band structure and density of states. We tested five types of different functionals to study the band structure and density of states of a single-layer *h*-BN. Small differences have been noticed regarding band structure and density of state details. Nevertheless, HSE03 deduced the band gap accurately within a 3.4% deviation from the experimental value compared with LDA which showed a 24.4% error.

Keywords: DFT; First principles; *H*-BN; Electronic structure; Band gap; Hybrid functional

1 Introduction

First-principles calculations based on density functional theory (DFT) often utilize the generalized gradient approximation (GGA) or local density approximation (LDA) exchange-correlation (XC)-functional to describe the ground electron states and related properties. Unfortunately, using LDA and GGA approximations significantly underestimate the energy band gap[1] although they predict many ground state properties with high accuracy and provide insight into mechanisms at the atomic level that determine the performance of the material at the macroscopic level[2]. Among the alternatives is to replace them with hybrid functionals such asBLY3P for molecules[3] and nonperiodic structures along with HSE06 and HSE03 prepared for periodic materials description which come with computationally additional cost.

Since the synthesis of graphene and being undoubtedly stable[4,5], there is a remarkable effort going on to study and fabricate hexagonal two-dimensional (2D) structures[6–8]. These atomically thin crystals started with graphene[9] but cover now many new members like silicene[10], hexagonal boron nitride (*h*-BN)[11], and transition metal dichalcogenides[12] represent an attractive family of materials that have been growing over the past decade[13]. The atoms in each layer of 2D materials are strongly bonded while the layers are attached to each other by weak Van der Waals forces[14]. Furthermore, they are characterized by a large passive surface area with no dangling bonds which may have potential applications with photonic structures[15]. Also, since 2D materials have different band structures and energy gaps they cover a wide range of electromagnetic spectra[16–19].

Hexagonal boron nitride (*h*-BN) has very similar to graphene (that's why it is called white graphene) it has a honeycomb structure, but instead, carbon atoms are replaced by Boron (B) and Nitrogen (N) atoms alternately arranged in an infinite hexagonal grid.[20]. B and N atoms are bonded to each other by a strong sp^2 covalent bond within the same layer, the bond length between neighboring B-N atoms is about 0.145 nm with lattice parameters $a = b = 0.254$ nm[21]. Therefore, the space between the atomic layers is large, ($c = 0.6661$ nm) and it is easy to slide on each other, making it easily mechanically exfoliated and producing a single or a few layers of *h*-BN much like

*Corresponding author: (E-mail: i.hassan@uokirkuk.edu.iq)

the graphene[22]. Although the monolayer *h*-BN has a very similar lattice structure to graphene with a lattice inconsistency of almost about 1.8% they have contradictory electrical conductivities. While graphene has a zero bandgap and is considered a semi-metal showing a good electrical conductivity *h*-BN is a wide-bandgap (about 6 eV depending on the number of layers) semiconductor and normally maybe considered an insulator[23].

h-BN shows fascinating physicochemical properties. Among these properties are mechanical strength, thermal stability, electrical insulation, high thermal conductivity, and chemical stability[24]. Recently *h*-BN has been attracting more attention with the emergence of 2D atomic crystals and van der Waals heterostructures[25]. It may be used as an outstanding dielectric within heterostructures because of its large bandgap and structural similarities with graphene[26].

Due to the extraordinary properties of *h*-BN, it has vast potential applications in many fields, including catalysis[27], electronic devices[28], optoelectronics[29], thermal management[30], protective coating[31], biomedical applications[32,33,34], energy storage[35,36], UV emitters[37] and optical devices[38].

Despite the growing interest, the questions about nature and the value bandgap are still attracting some attention. Experimentally, by means of optical spectroscopy, there is convincing evidence for an indirect bandgap at 5.955 eV[39]. Most of the DFT-based calculations that are using GGA-PBE XC functionals are underestimating the energy band gap and away from the reliable experimental values[40,41]. In this work, we are presenting an investigation of structural, phonon dispersion, and electronic properties using DFT-based CASTEP code. Five different exchange-correlation XC functionals that are implemented in CASTEP have been tested in describing the band gap and the results have been compared with the experimental value.

2 Computational Methods

All the calculations throughout the study including geometry optimization, phonon dispersion, and band structure calculations have been conducted by using the CASTEP code[42]. We carried out the geometry optimization and the phonon dispersion calculations by using GGA-PBE (XC) functionals. Even though Kohn-Sham DFT based on GGA functional undervalues the band gap it works quite well regarding the total energy description and materials equilibrium structure[43]. However, to understand the properties of semiconductors and insulators an accurate determination is required for electronic structures and band gap values. Hence, we used five types of (XC) potential functionals to calculate energy band structure, the density of states and deduce the band gap through this work:

1) Local density approximation (LDA) by means of CA-PZ which is proposed parameterization by Perdew and Zunger (1981) based on the numerical results of Ceperley and Alder (1980)[44,45].

2) The second type which is widely used nonlocal or gradient corrected functionals that depend on the density and its gradient that adds an additional cost versus the better accuracy. Generalized Gradient Approximation (GGA) is a group of functional, not a particular one. The nonlocal functionals available in CASTEP include Perdew-Burke-Enzerhof (PBE) [46] and PBE sol functional, which is supposed to give a better description for the gradient expansion over a wide range of density gradients of densely packed solids [47].

3) The third class is Hybrid functionals such as HSE03[48,49] and HSE06[50] which are non-local exchanges that can only be used for insulators. In this class, a portion of the exact exchange from the Hartree-Fock theory has been incorporated with the rest of the XC energy. This can make calculations more demanding regarding the CPU time and needed memory.

The most stable crystalline form of boron nitride is the hexagonal one which has a layered structure like graphene with a point group= D_{h6} and a space group= $P6_3/MMC$. Nevertheless, *h*-BN may exist in five distinct high-symmetry stackings of bilayer which leads to differences in many properties[51]. In the AA stacking the B atom sits directly on top of the B atom and N atom directly on N while in the most stable AA' stacking, the hexagonal rings also sit directly on each other, but the Band N atoms alternate along the c-axis. In the other three AB stackings, one layer is shifted within the basal plane so that half of the atoms sit on top of the empty hexagon centers. Since we are interested in a single layer of *h*-BN, the simplest AA stacking has been adopted with a large spacing between layers.

All the computations were carried out using the (3x3x1) super cell (embodies 25 atoms) as shown in Fig. 1. The distance between successive layers was set

to 30 A^{o} to prevent any interaction between neighboring layers and this way it may be considered as an isolated single layer. Taking symmetry accounts into consideration the actual calculations have been performed on a single primitive cell along with using a (7x7x1) grid for Monkhorst-Pack sampling of Brillouin zone (BZ)[52].

3 Results and Discussion

3.1 Structural and Dynamical Properties

The present work starts by choosing a supercell (3x3x1) which includes two atoms per primitive unit cell. The crystalline structure belongs to the hexagonal system with a space symmetry group P6/mmm (the crystal has a six-fold rotational symmetry about its c-axis and mirror symmetry with respect to the basal plane). All the atoms were optimized using DFT with PBE XC-functionals and the BFGS minimizer[53]. The main advantage of this method is the ability to perform cell optimization. The atomic coordinates were optimized until the force on each atom was less than 10^{-5}eV/Å. During the entire calculation, cut-off energy was kept at 517.0eV for reasonable accuracy. The final optimized structure is shown in Fig. 1. The optimized lattice parameters were a = b = 2.511 Å and the (B-N) bond length within the same layer was 1.45 Å while the bond angle (B-N-B) was 120^{o}. These values are in fine agreement with the reported practical and computational values[54,55].

The next step is to check the dynamical stability of the single-layer *h*-BN structure by plotting the phonon dispersion curve. The phonon in quantum mechanics is a quasi particle that represents an excited state quantization of the modes of vibration for elastic structure in a periodic arrangement of atoms or molecules in a condensed matter[56]. The phonon dispersion relations are defined as *k* dependence of the frequencies of normal modes for all branches in selected directions in the crystal. Since there are two atoms B and N in every primitive unit cell should be described by 6 coordinates. The secular equation to be solved will result in 6 branches. Phonon calculations are carried out using GGA-PBE XC-functionals. Fig. 2 shows the plotted phonon dispersion branches of *h*-BN. The phonon branches which originate from the Γ point of the Brillouin zone correspond to acoustic modes. Where (ZA) represents out-of-plane mode, (TA) represents in-plane transverse mode, and (LA) stands for in-plane longitudinal mode. The remaining three branches correspond to optical modes: one out-of-plane mode (ZO) and two in-plane modes (TO and LO). Due to the mirror symmetry of *h*-BN planes, the vibration modes in the Z direction are decoupled from the XY plane in which longitudinal acoustic mode (LA) and out-of-plane mode (ZO) do not couples with other phonon modes[57]. The branch of acoustic modes is decoupling from the rest revealing a tendency of BN to form ripples and deform out-of-plane. The other point that is noticeable is LO-TO optical modes splitting owing to the long-range interactions in *h*-BN layers.

3.2 Electronic Properties

We performed the electronic band structure and density of states along Γ-M-K-Γ high symmetry directions to study the electronic properties of *h*-BN. At this moment we tested five different XC-

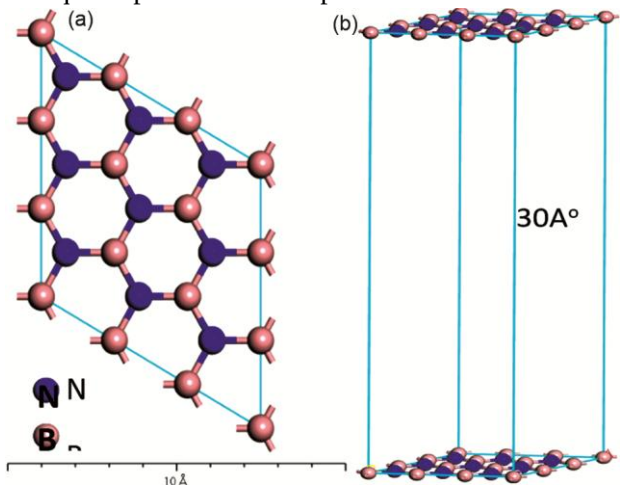

Fig. 1 — 3x3x1 supercell *h*-BN used in calculations where c has been taken 30A^{o} to ensure the absence of any interaction between neighboring layers (a) top view (b) side view.

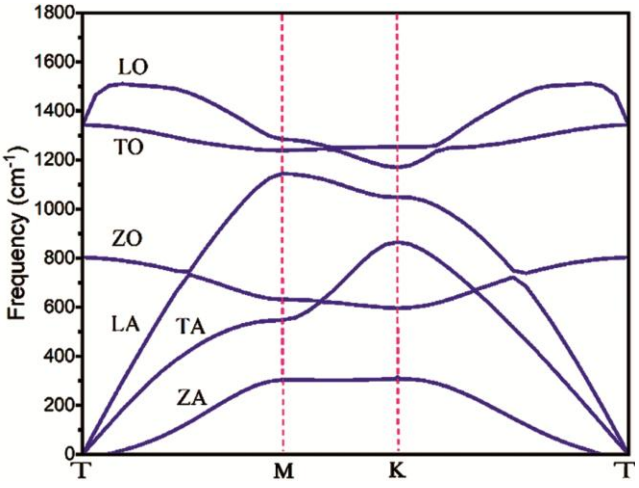

Fig. 2 — Phonon dispersion spectra of monolayer *h*-BN showing the three acoustic and optical bands along G-M K-G high symmetry path.

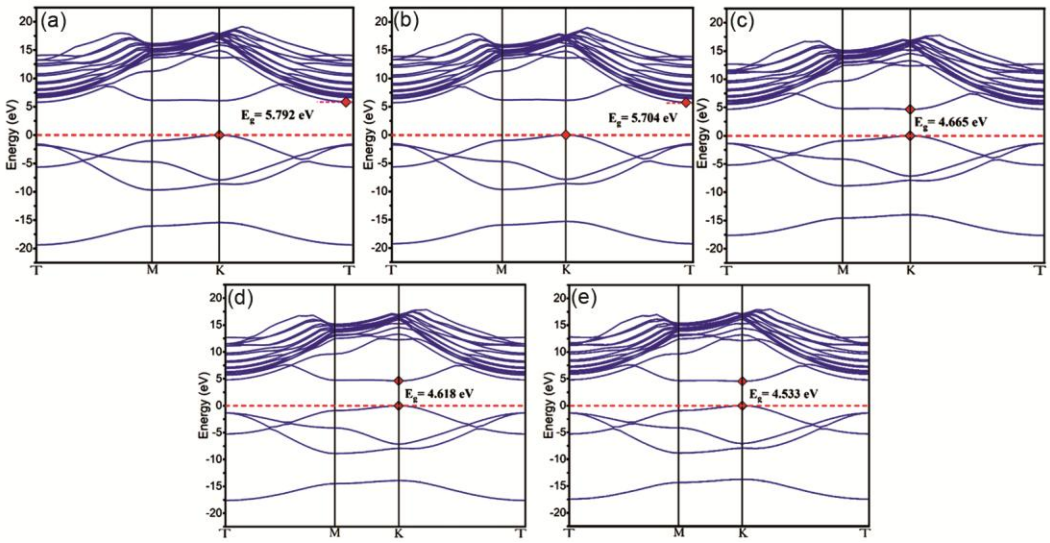

Fig. 3 — Band structure plotted along G-M-K-G high symmetry path for *h*-BN calculated by DFT based (a) HSE03 (b) HSE06 (c) GGA-PBE (d)GGA-PBESOL and (e) LDA XC-functionals. The red dashed lines indicate the Fermi level which is taken at the top of the valence band.

functionals available in CASTEP. Except for the HSE03 (where the cutoff energy has been set to 700.0eV for time-saving purposes) in all other cases, the cutoff energies have been set to 898.0 eV. While electron energy tolerance has been set to 10^{-6} in all calculations.

The resulting electronic band structures are shown in Fig. 3. Generally, it's clear the origin of poor conductivity of *h*-BN which is resulting from its wide band gap nature. That is why we may consider this material a wide band gap semiconductor or insulator. We notice that the maxima of valence bands are located at the K-point while the minima of the conduction bands are located at the G point for the band structures deduced using hybrid functionals HSE03 and HSE06 (Fig. 3(a,b)). This means that *h*-BN is an indirect band gap that agrees with practical results.

The best accurate band gap value was deduced by using HSE03 within a 3.4% deviation from the experimental value. However, the results by using the other two GGA and LDA XC-functional (Fig. 3(c-e)) led to a direct band gap at the K point with an error ranging from 22.2 to 23.4 %. It is noticeable that aside from the band gap value the energy band structures are very similar. The results have been tabulated in Table 1.

Table 1 — Comparison between the calculated energy band gap in (eV) using different X-C functionals compared with the experimental value.

	X-C-functional	band gap (eV)	Gap type	Deviation from exp. value %
Present work	HSE03	5.792	indirect	3.4
	HSE06	5.704	Indirect	4.9
	GGA-PBE	4.665	Direct	22.2
	GGA-PBESOL	4.618	Direct	23
	LDA-CA-PZ	4.533	Direct	24.4
Ref[39]	experimental	5.995	indirect	-

3.3 Density of States

As we mentioned earlier, we tested five different XC-functionals to determine the partial and total density of states (PDOS and TDOS) using five types of XC-functionals. The results are shown in (Fig. 4(a-e)). The DOS and projected DOS (PDOS) on both the B and N atom were conducted for the isolated single layer using each of the five XC functionals and were compared to each other. The obvious differences between the output from the five different XC-functionals types-based calculations are the different band gap values. The contributions of 2s and 2p states from boron and nitrogen atoms are shown in projected DOS graphs (PDOS) on the B and N atoms.

Regarding the total density of states (TDOS), the highest peaks take place in the conduction band mainly contributed by the B atom as is clearly seen from the PDOS of the boron atom. While the highest contribution in the valence band is from the 2p states of the N atom.

Several features are common to all functionals. First, the s and p peaks have overlapping energy ranges which clearly refers to the sp^2 hybridization in the valance (VB) and conduction bands (CB).Second,

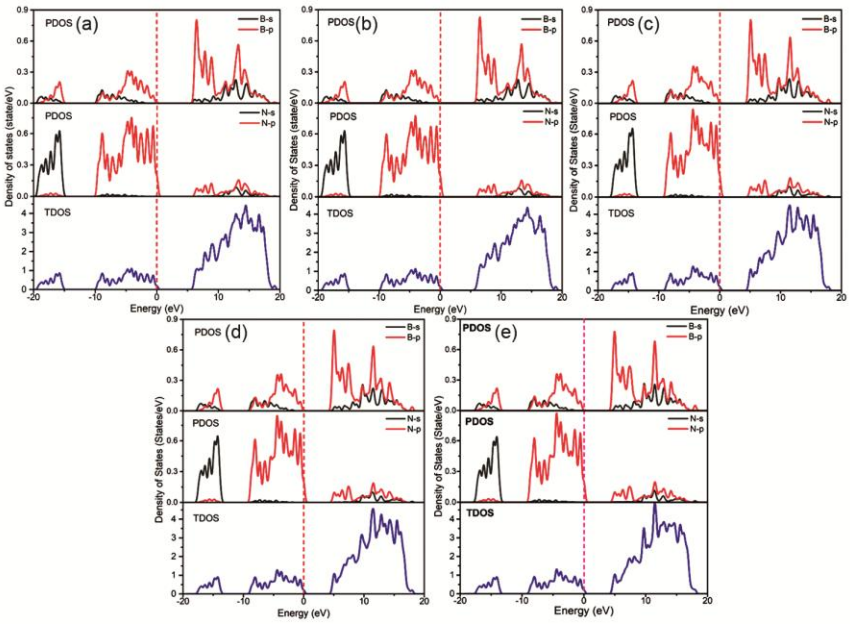

Fig. 4 — The partial density of states PDOS projected on B and N atoms compared with the total density of states (TDOS) using different XC-functionals-based calculations: (a) DFT-HSE03 (b) DFT-HSE06 (c) DFT-GGA-PBE (d) DFT-GGA-PBESOL (e) DFT-LDA.

we notice from PDOS of N that p peaks are higher in the VB and weaker in the core levels. This means that the N core state is comprised of 1s electrons with minimal p character. In the VB, N has five valance electrons, and the extra electron it withdraws from adjacent B atoms goes into 2p orbitals, hence raising the 2p peaks in the VB.Also, from the PDOS it is obvious that the band gap between CB and the VB on both B and N atoms is determined by the 2p and 3p orbitals peaks respectively. This means that the most likely electronic excitation in *h*-BN is from 2p orbital to 3p orbital.

There are small differences in PDOS deducted by different XC functionals. The most noticeable feature is the peaks in the B PDOS are almost the same for all XC functionals except for the obvious shifting in their positions especially for hybrid functionals HSE06 and HSE03. This is not true for the N PDOS where the height and positions of the VB peaks are getting lower and closer to each other as we go from LDA to HSE03 results. Furthermore, the core levels stand in the range of 0 to -20eV for hybrid functionals while they are in the range of 0 to about 18eV for the rest of the other three functionals.

4 Conclusions

We investigated the structural geometry, stability, and electrical properties of a single-layer *h*-BN. Five types DFT based XC-functionals implemented in CASTEP code have been tested to deduce the band structure and density of states. The absence of imaginary modes in the phonon dispersion curve shows its dynamical stability. The branch of acoustic modes is decoupling from the rest, revealing BN's tendency to form ripples and deform out-of-plane. The most accurate band gap was deduced by using hybrid functionals. The best value was 5.792 eV, an indirect gap between K and Γ points using HSE03 functionals with only a 3.4% deviation from the experimental results. While the biggest underestimation of the bandgap resulted from using LDA with a deviation of 24.4% from the experimental value. The wide band gap means it is an insulator at room temperature. Thus, *h*-BN has great importance in optoelectronic applications such as UV detectors, transparent electrodes, and UV light-emitting diodes. Regarding the total density of states (TDOS), the highest peaks take place in the conduction band mainly contributed by the B atom as is clearly seen from the PDOS of the boron atom. While the highest contribution in the valence band is from the 2p states of the N atom. In future, we hope to study the impact of using different XC functionals on optical properties and electronic transitions.

References

1 Munef R A, Ghaleb A M & Shihatha A T, *Tikrit J Pure Sci*, 26 (2021) 75.
2 Kohn W & Sham L J, *Phys Rev*, 140 (1965) A1133.
3 Hassan I Z Aydin M & Jalal S, *AIP Conf Proc*, 2213 (2020).
4 Geim A K & Novoselov K S, *Nature Materials*, 6 (2007) 183.

5 Kim K S, *et al., Nature*, 457 (2009) 706.
6 Novoselov K S, *et al.* www.pnas.orgcgi (2005), doi10.1073pnas.0502848102.
7 Kharadi M A, *et al., ECS J Sol State Sci Technol*, 9 (2020) 115031.
8 Malyi O I, Sopiha K V & Persson C, *ACS Appl Mater Interf*, 11 (2019) 24876.
9 Ferrari A C, *et al., Nanoscale*, 7 (2015) 4598.
10 Oughaddou H, *et al., Prog Surf Sci*, 90 (2015) 46.
11 Pakdel A Bando Y & Golberg D, *Chem Soc Rev*, 43 (2014) 934.
12 Li H, Shi Y, Chiu M H & Li L, J *Nano Energy*, 18 (2015) 293.
13 Banks C E & Brownson D A C *2D Mater*, (2018).
14 Xu M, Liang T, Shi M & Chen H, *Chem Rev*, 113 (2013) 3766.
15 Abed H H, *et al.,* (2022) doi:10.21203/rs.3.rs-1999342/v1.
16 Kianinia M, Xu Z Q, Toth M & Aharonovich I, *Appl Phys Rev*, 9 (2022). https://doi.org/10.1063/5.0072091.
17 Zhao M, *et al., Crystals*, 12 (2022) https://doi.org/10.3390/cryst12081087.
18 Vatanparast M & Shariatinia Z, *J Mol Graph Model*, 89 (2019) 50.
19 Wu J, *et al., Mater Today Energy*, 28 (2022) 101065.
20 Zhang K, Feng Y, Wang F, Yang Z & Wang J, *J Mater Chem C*, 5 (2017) 11992.
21 Nag A, *et al., ACS Nano*, 4 (2010) 1539.
22 Kim D, Lee Y, Chacón A & Kim D E, *Symmetry (Basel)*, 14 (2022).
23 Hassan I Z & Ali E M, *Turkish J Comput Math Educat*, 12 (2021) 1269.
24 Malozovsky Y, Bamba C, Stewart A, Franklin L & Bagayoko D, *J Mod Phys*, 11 (2020) 928.
25 Paleari F, *et al., 2D Mater*, 5 (2018) 045017.
26 Casiano-Jiménez G, Ortega-López C, Rodríguez-Martínez J A, Moreno-Armenta M G & Espitia-Rico M J, *Coatings*, 12 (2022).
27 Zhang X, Kang L & Zhu M, *Int J Mol Sci*, 23 (2022) 9997.
28 Dean C R, *et al., Nature Nanotechnol*, 5 (2010) 722.
29 Ogawa S Fukushima S & Shimatani M, *Materials*, 16 (2023).
30 Wang Y, *et al., Nanoscale*, 10 (2017) 167.
31 Yang X, Zhang R, Pu J, He Z & Xiong L, *Corrosion Rev*, 39 (2021) 93.
32 Chen Y, Tan C, Zhang H & Wang L, *Chem Soc Rev*, 44 (2015) 2681.
33 Li Y, *et al., RSC Adv*, 9 (2019) 29805.
34 Safari L, Vessally E, Bekhradnia A, Hosseinian A & Edjlali L, *Thin Solid Films*, 623 (2017) 157.
35 Chettri B, Patra P K, Hieu N N & Rai D P, *Surf Interf*, 24 (2021).
36 Fartab D S & Kordbacheh A A, *Superlattices Microstruct*, 118 (2018) 185.
37 Li S, Pershin A, Thiering G, Udvarhelyi P & Gali A, *J Phys Chem Lett*, 13 (2022) 3150.
38 Abed H H, *et al.* (2022) doi:10.21203/rs.3.rs-1999342/v1.
39 Cassabois G, Valvin P & Gil B, *Nat Photon*, 10 (2016) 262.
40 Niraula P, *Dissertations, Theses, and Capstone Projects* (2020).
41 Beiranvand R &Valedbagi S, *Optik (Stuttg)* 127 (2016) 1553.
42 Clark S J *et al., Zeitschrift fur Kristallographie*, 220 (2005) 567.
43 Pelá R R*et al., Appl Phys Lett*, 98 (2011) 151907.
44 Ceperley D M & Alder B J, *Phys Rev Lett*, 45 (1980) 566.
45 Perdew J P & Zunger A, *Phys Rev B*, 23 (1981) 5048.
46 Perdew J P, Burke K & Ernzerhof M, *Phys Rev Lett*, 77 (1996) 3865.
47 Perdew J P, *et al., Phys Rev Lett*, 100 (2008) 136406.
48 Heyd J, Scuseria G E & Ernzerhof M, *J Chem Phys*, 118 (2003) 8207.
49 Heyd J & Scuseria G E, *J Chem Phys*, 121 (2004) 1187.
50 Krukau A V, Vydrov O, AIzmaylov A F & Scuseria G E, *J Chem Phys*, 125 (2006) 224106.
51 Latil S, Amara H & Sponza L *Sci Post Phys*, 14 (2022) 53.
52 Wang Y, Wisesa P, Balasubramanian A, Dwaraknath S & Mueller T, *Comput Mater Sci*, 187 (2021) 110100.
53 Pfrommer B G, Côté M, Louie S G & Cohen M L, *J Comput Phys*, 131 (1997) 233.
54 Ooi N, Rajan V, Gottlieb J, Catherine Y & Adams J B, *Model Simul Mat Sci Eng*, 14 (2006) 515.
55 Usachov D, *et al., Phys Rev B Condens Matter Mater Phys*, 86 (2012) 155151.
56 The Oxford Solid State Basics | University of Oxford Podcasts. https://podcasts.ox.ac.uk/series/oxford-solid-state-basics.
57 Anees P, Valsakumar M C & Panigrahi B K, *Phys Chem Chem Phys*, 18 (2016) 2672.